Modified Preisach Model of Hysteresis in Multi Air Gap Ferrite Core Medium Frequency Transformer

Michał Michna, *Senior Member, IEEE*, Piotr Dworakowski, *Senior Member, IEEE*, Andrzej Wilk, *Member, IEEE*, Filip Kutt, and Michel Mermet-Guyennet

***Abstract*—This article presents the modified Preisach model of hysteresis for a 3-phase medium frequency transformer in a 100 kW dual active bridge converter. The transformer magnetic core is assembled out of ferrite I-cores, which results in multiple parasitic air gaps. For this transformer, the hysteresis loops were measured and the parameters of the Preisach model were determined. The Preisach distribution function is approximated with a two-dimensional Gauss function series and the feedback function is a 3rd-degree polynomial. The optimized identification of Preisach distribution function parameters was prepared. Two sets of parameters were determined based on the analysis of major and minor hysteresis loop. The developed model is used to analyze the transformer core power loss. A new set of Steinmetz equation parameters for the multi air gap ferrite core MFT is proposed.**

***Index Terms*—Ferrite core, gapped magnetic core, hysteresis loop, medium frequency transformer, power loss, Preisach model, Preisach distribution function.**

I. Introduction

THE medium frequency transformer (MFT) is one of the key components of the isolated dc-dc converters. The isolated dc-dc converter is the enabling technology in modern electrical power systems and transportation applications where the galvanic separation is required. The isolated dc-dc converter topologies suitable in high power applications include series resonant converter [1], LLC dc-dc resonant converter [2], phase-shifted full bridge [3], single active bridge [4] and dual active bridge (DAB) [5]. The 3-phase DAB is considered in the applications where the high power density and high efficiency are required [6], [7].

The MFT is still quite a novel technology with lots of research interest. Some designs of high power MFT were reported in [8]–[11]. The ferrite core is considered for medium and high frequency transformers due to its low power loss and low material cost compared to amorphous and nanocrystalline [12], [13]. The high power ferrite MFT requires the construction of the magnetic core using type "I" cores which results in multiple parasitic air gaps [14], [15].

The mathematical model of the transformer as a component of power systems was presented in many papers. The 50/60 Hz transformer modeling has been extensively studied for the electromagnetic transient simulations [16]–[19]. On the other hand, MFT modeling has to take into account the high frequency effects on the winding resistance [20], [21], parasitic capacitances [22], [23], and core loss [24], [25]. A nonlinear model of a 3-phase MFT was proposed in [26]. The precise MFT design and modeling should consider a time-dependent model of the magnetic hysteresis.

The macroscopic models of hysteresis are reviewed in [27] and they are considered the most suitable in finite element and equivalent circuit modeling. In the equivalent circuit modeling, the hysteresis nonlinearity can be involved directly in the function $\Phi(\Theta)$ [28] or indirectly through the coupled equivalent reluctance model and the function $B(H)$ [29]. Several macroscopic hysteresis modes have been developed. These include Tellinen [30], Stoner-Wolhfart [31], Globus [32], Jiles-Atherton [33], and Preisach [34]. The Jiles-Atherton model and the Preisach model have shown very high accuracy. The modifications [35], [36] of those models are the most accurate. The Jiles-Atherton model is based on the magnetization reversible and irreversible components. It can be used in the analysis of hysteresis phenomena in several physical domains [37]–[39]. A mathematical form of the Preisach model (PM) was developed in [40], [41]. This model is based on a two-dimensional integral of Preisach distribution function (PDF). The original PM was subject to some modifications which are reviewed in [36]. The PM modifications include: generalized PM, moving PM, dynamic PM, vector PM and feedback PM. The classical PM does not represent precisely the minor hysteresis loops due to the congruency property [42], [43]. The feedback Preisach model (FPM) allows removing the congruency property. This PM modification has been selected and it is further developed in this article.

To use the Preisach hysteresis model in a simulation, it is necessary to define the PDF and to determine its parameters [44]–[49]. A variety of functions were used to define PDF, including a Factorized-Lorentzian, a Gauss, or a Lognormal-Gauss distribution function [49]. In [50], [51] the Preisach model

Manuscript received September 14, 2020; revised December 14, 2020; accepted January 20, 2021. Date of publication January 25, 2021; date of current version January 24, 2022. This work was supported by the French National Research Agency (ANR) as part of the "Investissements d'Avenir" Program (ANE-ITE-002-01) and the LINTE^2 Laboratory at the Gdansk University of Technology. *(Corresponding author: Michał Michna.)*

Michał Michna, Andrzej Wilk, and Filip Kutt are with the Faculty of Electrical and Control Engineering, Gdańsk University of Technology, 80-233 Gdansk, Poland (e-mail: andrzej.wilk@pg.edu.pl; michal.michna@pg.edu.pl; filip.kutt@pg.edu.pl).

Piotr Dworakowski and Michel Mermet-Guyennet are with the Power Electronics and Converters, SuperGrid Institute, 69100 Villeurbanne, France (e-mail: piotr.dworakowski@supergrid-institute.com; michel.mermet-guyennet@alstomgroup.com).

Color versions of one or more figures in this article are available at https://doi.org/10.1109/TPWRD.2021.3054059.

Digital Object Identifier 10.1109/TPWRD.2021.3054059

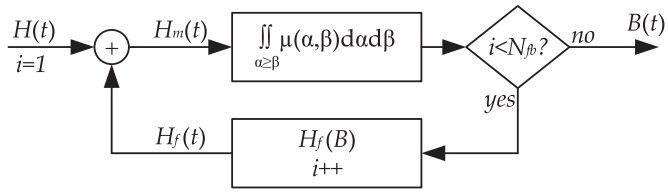

Fig. 1. Feedback Preisach model of a hysteresis block diagram.

was implemented in a circuit simulation of an isolated dc-dc converter with a single-phase transformer.

This article presents the modified Preisach model of hysteresis for a 3-phase MFT in a 100 kW DAB converter. The Preisach distribution function is approximated with a two-dimensional Gauss function series (2DGFS) and the feedback function is a 3rd-degree polynomial. The developed model is used to analyze the MFT core power loss. The original contribution of this paper include:

- demonstration that the feedback Preisach model of hysteresis accurately represents the magnetic hysteresis loops in the multi air gap medium frequency transformers composed of type "I" ferrite cores in the aspect of power loss calculation,
- analysis of the model accuracy considering separate parameters of 2DGFS for the major and minor magnetic hysteresis loops,
- analysis of the model accuracy as the function of the number of terms in the 2DGFS and the number of feedback loop iterations,
- determination of Steinmetz equation parameters for calculating power losses in the multi air gap MFT composed of type "I" ferrite cores.

The feedback Preisach model is developed in Section II. Section III presents the measurement of the equivalent $B(H)$ for the 3-phase MFT prototype involving multiple parasitic air gaps. Section IV presents the calculation of feedback Preisach model parameters. Section V analyses the MFT core power loss using the proposed hysteresis model.

II. Feedback Preisach model of Hysteresis

The magnetic materials are characterized by the nonlinear relationship $B(H)$ between the magnetic flux density B and the magnetic field strength H. The $B(H)$ relationship is history-dependent. The shape of the $B(H)$ depends on the material properties and the maximum value of H. The hysteresis has a significant effect on the analysis of the transformer inrush, magnetic core remanence, resonant circuits involving a transformer and core power loss.

The feedback Preisach model (FPM) block diagram is presented in Fig. 1. The upper block represents the classical Preisach model with the two-dimensional integral of the Preisach distribution function (PDF) $\mu(\alpha, \beta)$. The lower block represents the feedback function $H_f(B)$ where the number of iterations N_{fb} can be freely selected.

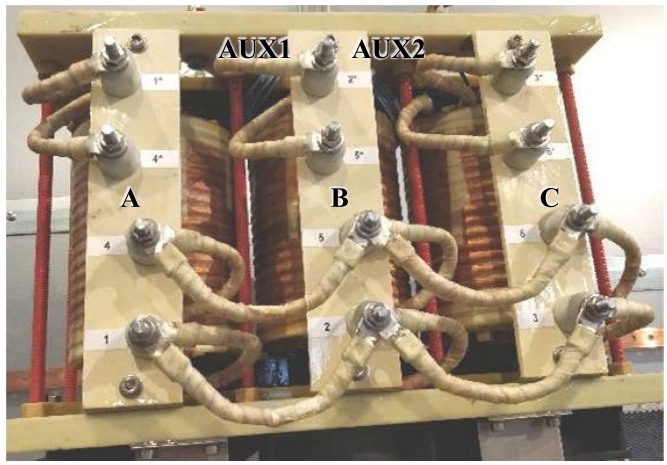

Fig. 2. Medium frequency transformer prototype with three columns A, B, C, and auxiliary coils AUX1 and AUX2.

The feedback Preisach model (FPM) is defined as:

$$B(t) = \iint_{\alpha\geq\beta} \mu\left[\alpha + H_f(B), \beta + H_f(B)\right] \gamma_{\alpha,\beta} \times \left[H + H_f(B)\right] d\alpha d\beta \quad (1)$$

where $\mu(\alpha,\beta)$ is the PDF of the classical Preisach Model (PM), $\mu(\alpha + H_f(B), \beta + H_f(B))$ is the PDF of the FPM with the feedback function $H_f(B)$, $\gamma_{\alpha,\beta}(H)$ is the hysteresis operator of the classical PM with randomly distributed parameters α and β, $\gamma_{\alpha,\beta}(H + H_f(B))$ is the hysteresis operator of the FPM.

The PDF $\mu(\alpha, \beta)$ and the feedback function $H_f(B)$ need to be defined for the FPM to be implemented. In the presented research the PDF is approximated by an N_{fs}-term two-dimensional Gauss function series and the feedback function is approximated by a 3rd-degree polynomial:

$$\mu(\alpha,\beta) = \frac{1}{2\pi} \sum_{n=1}^{N_{fs}} \frac{A_n}{S_{x,n} S_{y,n}} \exp\left(\frac{-(\alpha+\beta)^2}{2{S_{x,n}}^2}\right) \times \exp\left(\frac{-(\alpha-\beta)^2}{2{S_{y,n}}^2}\right), \quad (2)$$

$$H_f(B) = K_1 B + K_3 B^3, \quad (3)$$

where A_n, $S_{x,n}$, $S_{y,n}$, K_1 and K_3 are constants defining the approximated function, α and β are the parameters of the hysteresis operator $\gamma_{\alpha,\beta}(H)$. The constants are phenomenological and they do not have any exact physical meaning.

III. Equivalent $B(H)$ Measurement

In order to calculate the FPM parameters $A_n, S_{x,n}, S_{y,n}, K_1, K_3$ as well as N_{fs} and N_{fb}, first, a measurement of the $\Phi(\Theta)$ or $B(H)$ is required. The $\Phi(\Theta)$ is useful in equivalent circuit simulations and $B(H)$ is useful in finite element method (FEM) simulations. The MFT prototype presented in Fig. 2 and detailed in [52] was used for the measurement and parameters estimation. Ferrite I-cores are used for the MFT magnetic core as shown in Fig. 3.

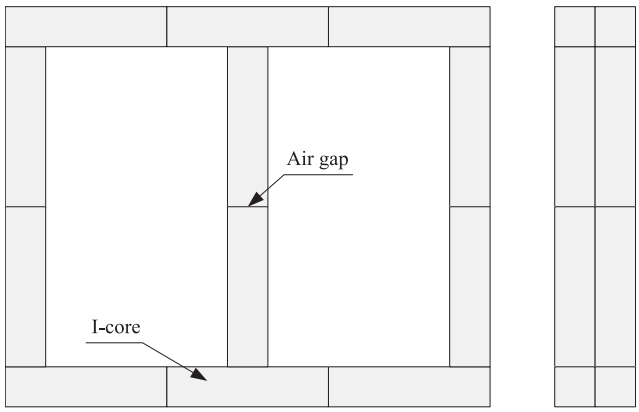

Fig. 3. Medium frequency transformer core assembly with multiple parasitic air gaps.

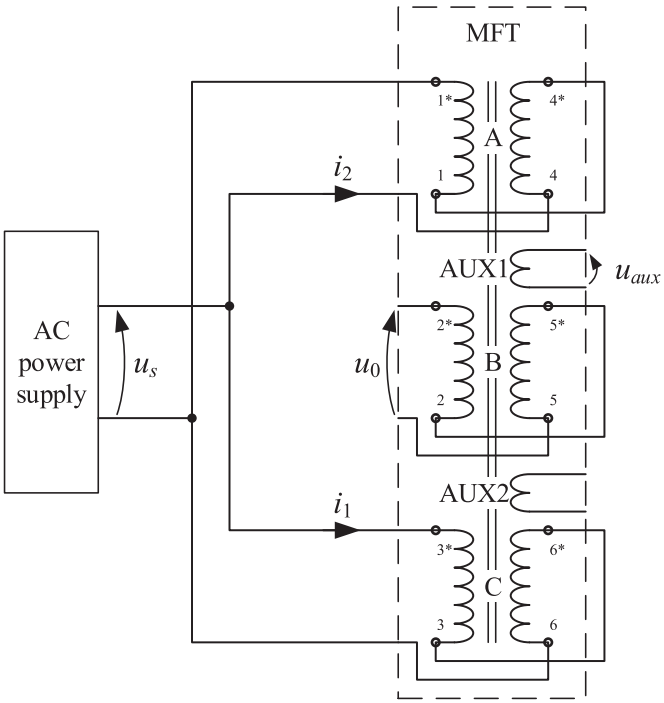

Fig. 4. Equivalent static $B(H)$ measurement setup circuit diagram.

The dimensions of I-cores vary from one sample to another causing the non-uniform parasitic air gaps in the core. These parasitic air gaps have unpredictable dimensions which leads to lower accuracy of the model. However, the homogenization of core material properties [53]–[55] can be applied. The authors proposed in [15] an empirical scaling function allowing an estimation of the average air gap length in the multi air gap ferrite core MFT. The effective magnetic permeability of gapped magnetic cores is discussed in [15], [56].

Based on the method proposed in [57] and detailed by the authors in [15] a static equivalent $B(H)$ measurement setup was developed. The circuit diagram is presented in Fig. 4 and the test bench implementation in Fig. 5.

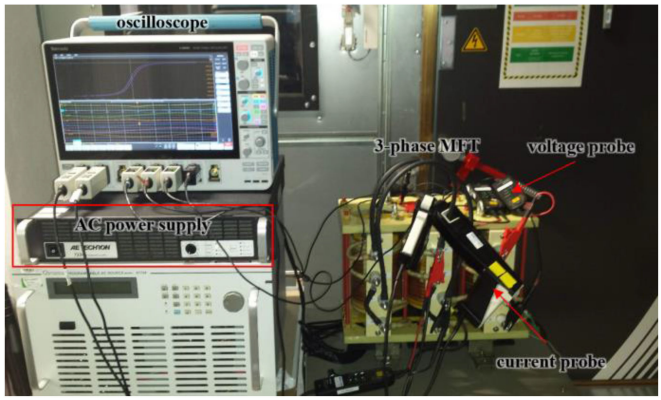

Fig. 5. Equivalent static $B(H)$ measurement setup implementation.

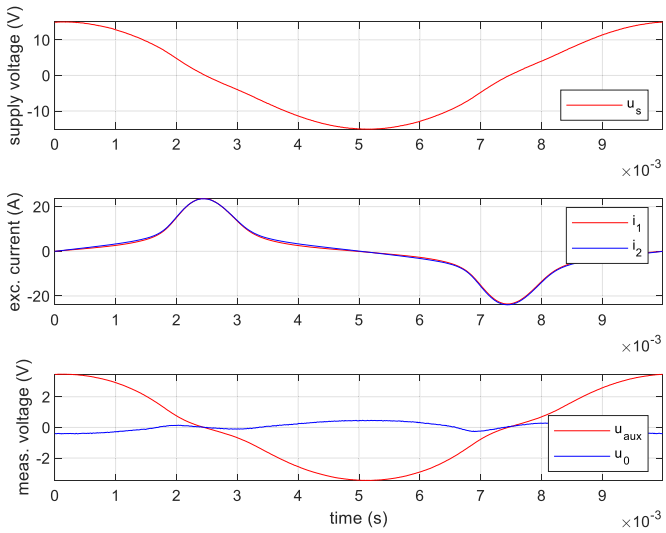

Fig. 6. Measured waveforms: supply voltage u_s, excitation currents i_1 and i_2, auxiliary coil voltage u_{aux} and remaining winding voltage u_0.

The transformer windings were connected in such way as to achieve a high magnetomotive force. The measurement of the magnetic flux in the core was achieved by placing two additional auxiliary coils on the yoke. In order to minimize the effect of eddy currents and residual losses, and to achieve good performance of the available power supply, the frequency of the power supply was set to 100 Hz. The measurement was performed at a constant core temperature 25 °C. The measured waveforms are shown in Fig. 6. The supply voltage is close to sinusoidal and the currents in two excitation windings are equal. The nonsinusoidal character of the currents is indicating the core saturation. The voltage amplitude of the central column winding (u_0) is relatively low. Based on the transformer dimensions, the magnetic field strength H and the magnetic flux density B can be calculated considering some simplifications. These simplifications include: constant core cross section, constant distribution of the magnetic flux density, average magnetic circuit length, neglecting the fringing effect, neglecting the magnetic flux coupling in the air and neglecting the magnetic flux in the central column (Φ_0).

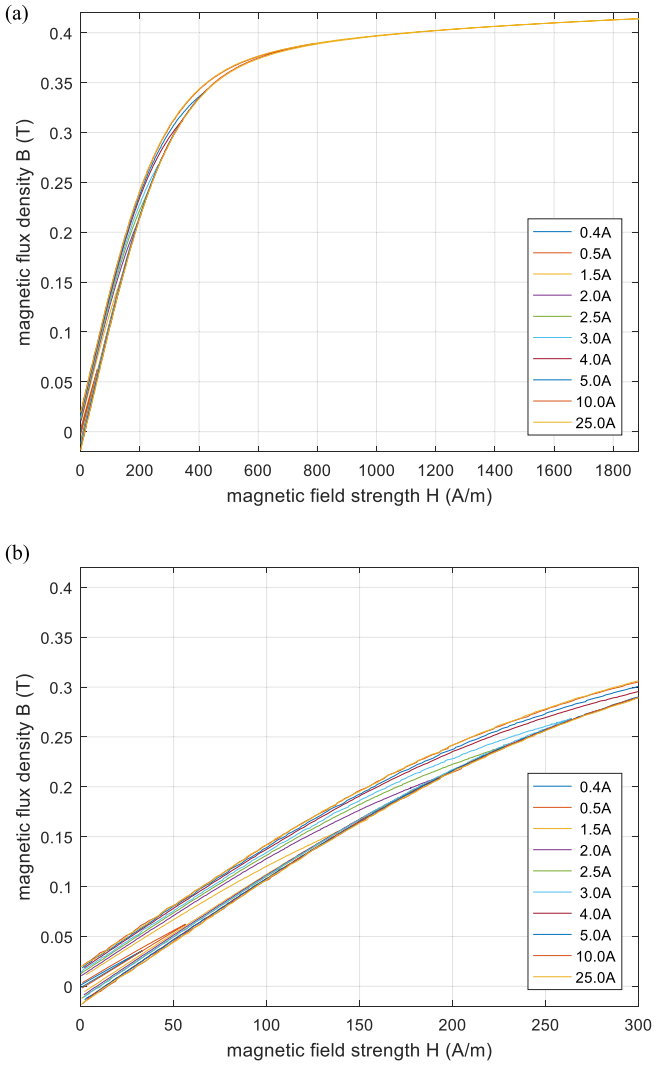

Fig. 7. Measured equivalent static $B(H)$ at 25 °C with different excitation current amplitudes: plot up to 1900 A/m (a) and plot up to 300 A/m (b).

A series of measurements were performed with different excitation current amplitudes corresponding to the magnetic field strength amplitude from 35 A/m to 1900 A/m. It was found that above 800 A/m the width of the hysteresis loop does not change significantly. The selected measured static hysteresis loops are presented in Fig. 7 for positive values of magnetic field strength. The coercive field H_c and remanent flux density B_r can be captured, which are 15 A/m and 20 mT, respectively. These values are consistent with the material datasheet [58] considering that the datasheet was realized according to IEC 62044 [59]. The datasheet $B(H)$ was measured on a ring core without any air gaps at 10 kHz. The influence of the temperature on the $B(H)$ is not analyzed in this article. The major loop and the minor loops of hysteresis were used to identify Preisach model parameters.

IV. Hysteresis Model Parameters

An analysis was carried out to determine the optimal number of terms of the approximating PDF series N_{fs} and a number

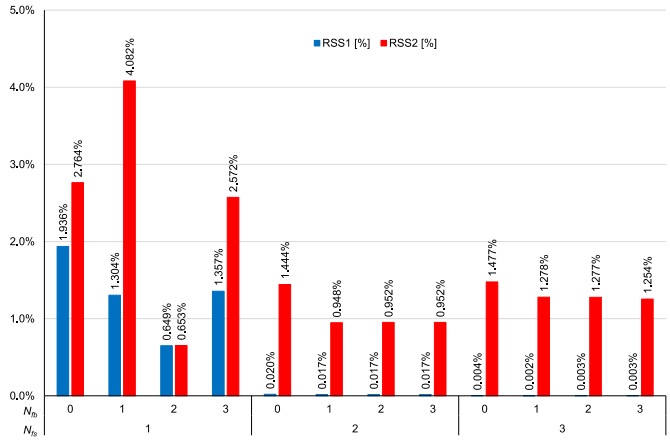

Fig. 8. Relative residual sum of squares (RSS) of Preisach hysteresis model for parameters determined based on the major hysteresis loop in function of the number of terms of the series N_{fs} and the number of feedback iterations N_{fb}: RSS1 is the error between simulation and measurement of the major hysteresis loop (blue) and RSS2 is the error between simulation and measurement of the minor hysteresis loop (red).

of feedback loops N_{fb}. In order to calculate the parameters A_n, $S_{x,n}$, $S_{y,n}$, K_1 and K_3 the trust-region reflective least-squares optimization algorithm with constraints [60] was used. The same set of initial parameters was used to identify the parameters of all PDF functions. The relative residual sum of squares (RSS) was used to compare results and defined as:

$$RSS = \frac{\sum (f_{sim} - f_{meas})^2}{\max (f_{meas})}, \tag{4}$$

where: f_{sim}– simulation results, f_{meas}– measurement results.

The values of the hysteresis model parameters determined based on the major loop are presented in Table I. RSS1 is calculated to estimate the error between simulation and measurements of the major hysteresis loop, and RSS2 is calculated for the simulated minor hysteresis loop. The relative RSS1 and RSS2 errors as a function of N_{fs} and N_{fb} are also shown in Fig. 8.

The values of the hysteresis model parameters determined based on the selected minor loop are presented in Table II.

For the major loop, the best fit is obtained for the PDF described by parameters $N_{fs} = 3$ and $N_{fb} = 1$ (Fig. 9(a)), which means using three terms of the Gauss series and one feedback loop iteration. However, it can be seen that slightly worse accuracy is also obtained for the PDF described by two elements of series, which is faster and less computer time-consuming. It is possible to use parameters determined based on a major hysteresis loop to simulate minor loops (Fig. 9(b)). In this case, the major hysteresis loop will be mapped accurately, and in the case of a minor loop, the RSS will increase by an average of about 8 times.

To increase the accuracy of the simulation of the minor hysteresis loop, the parameters of the PDF were determined based on the measurement of this loop (Table II). In this case, the lowest RSS value is obtained for the $N_{fs} = 2$ and $N_{fb} = 2$. Using these parameters ensures a very good accuracy of fitting of the minor hysteresis loop (Fig. 10(b)). On the other hand,

TABLE I
FEEDBACK PREISACH MODEL PARAMETERS DETERMINED BASED ON THE MAJOR LOOP FOR DIFFERENT NUMBER OF TERMS OF THE SERIES N_{fs}, AND NUMBER OF FEEDBACK ITERATIONS N_{fb}

N_{fs}	N_{fb}	$S_{x,1}$	$S_{x,2}$	$S_{x,3}$	$S_{y,1}$	$S_{y,2}$	$S_{y,3}$	A_1	A_2	A_3	K_1	K_3	RSS1	RSS2
1	0	539.5			38.37			1.60					1.936%	2.764%
	1	569.8			10.63			1.61			313.1	-2988.9	1.304%	4.082%
	2	503.3			42.76			1.62			83.2	-5232.8	0.649%	0.653%
	3	560.9			15.27			1.61			267.4	-2828.5	1.357%	2.572%
2	0	1623.3	443.0		32.90	38.71		0.32	1.34				0.020%	1.444%
	1	1667.6	450.9		29.50	34.68		0.31	1.35		31.6	-203.2	0.017%	0.948%
	2	1665.7	450.6		28.47	34.83		0.31	1.35		30.0	-182.3	0.017%	0.952%
	3	1665.6	450.6		28.48	34.84		0.31	1.35		30.0	-182.1	0.017%	0.952%
3	0	818.2	416.8	3017.9	55.03	36.28	5.34	0.34	1.15	0.21			0.004%	1.477%
	1	820.4	414.8	3143.3	22.16	40.81	9.14	0.36	1.13	0.22	-1.79	213.4	0.002%	1.278%
	2	840.1	418.3	3140.0	27.60	39.49	6.63	0.34	1.15	0.21	1.16	153.3	0.003%	1.277%
	3	853.0	421.1	3071.6	28.59	38.88	9.59	0.32	1.17	0.21	3.70	116.2	0.003%	1.254%

TABLE II
FEEDBACK PREISACH MODEL PARAMETERS DETERMINED BASED ON THE MINOR LOOP FOR DIFFERENT NUMBER OF TERMS OF THE SERIES N_{fs}, AND NUMBER OF FEEDBACK ITERATIONS N_{fb}

N_{fs}	N_{fb}	$S_{x,1}$	$S_{x,2}$	$S_{x,3}$	$S_{y,1}$	$S_{y,2}$	$S_{y,3}$	A_1	A_2	A_3	K_1	K_3	RSS1	RSS2
1	0	444			24.15			1.42					39%	0.156%
	1	463			27.35			1.48			107.2	-3914.4	22%	0.089%
	2	462			27.44			1.48			104.2	-4012.9	20%	0.090%
	3	462			27.45			1.48			105.4	-4025.7	21%	0.089%
2	0	1 695	344		0.03	40.90		1.90	0.72				440%	0.073%
	1	1 993	382		0.91	38.16		1.54	0.94		45.8	-2745.1	201%	0.067%
	2	3 591	458		26.85	27.73		0.01	1.47		85.5	-3677.3	21%	0.090%
	3	2 331	363		0.93	41.03		2.07	0.86				395%	0.065%
3	0	9 707	421	2 035	29.71	34.72	10.79	0.01	1.11	1.05			102%	0.338%
	1	21 536	451	1 924	30.02	30.66	10.81	0.05	1.15	1.05	27.04	-333.4	148%	0.273%
	2	22 355	374	1 965	30.00	31.82	5.95	0.01	0.86	1.73	26.60	-299.6	377%	0.096%
	3	22 373	352	1 965	30.00	35.47	4.59	0.00	0.75	2.08	26.41	-299.6	608%	0.081%

parameter sets developed based on minor loop measurements are not suitable for simulating a major hysteresis loop (Fig. 10(a)). If the precision of the model based on the major loop parameters is not sufficient then the parameters should be changed between the major or minor hysteresis loops.

V. ANALYSIS OF CORE POWER LOSS

The proposed feedback Preisach model can be further implemented in an equivalent circuit simulation allowing to evaluate the hysteresis power loss in transient and steady-state simulations, and to represent precisely the magnetizing current waveforms. In [50], [51], [61] the Preisach model was implemented in the circuit simulation of a single-phase transformer. In this section, the developed FPM is used in the analysis of core power loss and the circuit implementation of the hysteresis model for the 3-phase transformer will be reported in the future.

The core power loss P_c includes 3 components: hysteresis power loss P_h, eddy current effect power loss P_e and residual (or anomalous) power loss P_r. The eddy current effect power loss is neglected here because the ferrite conductivity is very low [58]. The authors have verified that at 20 kHz P_e accounts for approximately 1–2% of the total core power loss. In [62] the P_e is claimed below 10% at 100 kHz. The residual power loss is neglected as well. According to [62] at a fixed frequency the residual power loss P_r is proportional to hysteresis loss P_h. The ratio P_r/P_h is a linear function of frequency. At high frequency, the P_r can be a few times higher than P_h. However, at 20 kHz the ferrite residual power loss is expected to be low. The hysteresis power loss can be calculated for the operating frequency f and core volume V_c by measuring the surface of the $B(H)$ loop A_{BH}:

$$P_h = A_{BH}\, f V_c \tag{5}$$

The hysteresis power loss P_h was calculated for the measured $B(H)$ from Fig. 7 and using (5). Moreover, for each $B(H)$ from Fig. 7 the separate hysteresis model parameters were calculated according to Section IV. Then, using (5) the corresponding hysteresis power losses P_h were calculated. In Fig. 11 the hysteresis power loss is plotted in the function of magnetic flux density. The hysteresis power losses calculated based on measured and simulated $B(H)$ are compared. Power losses calculated using the separate hysteresis model parameters show a good fit to the measurement. Power losses calculated using the hysteresis model

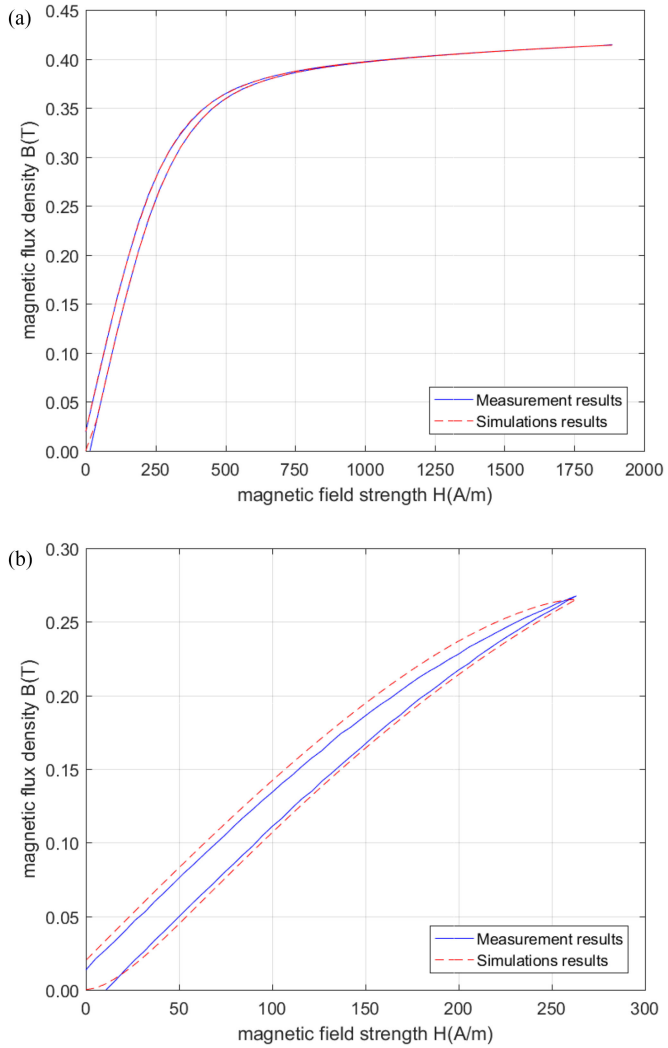

Fig. 9. Simulated and measured trajectories of the major hysteresis loops (a) and the minor hysteresis loops (b) for PDF model fitted to major loop with parameters $N_{fs} = 3$ and $N_{fb} = 1$.

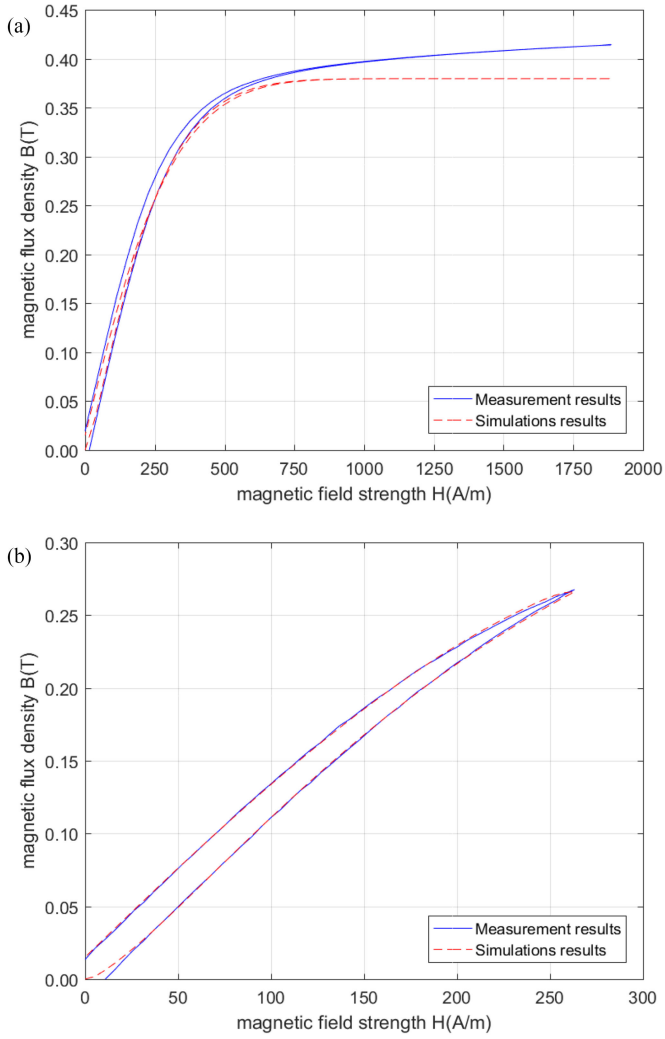

Fig. 10. Simulated and measured trajectories of the major hysteresis loops (a) and the minor hysteresis loops (b) for PDF model fitted to minor loop with parameters $N_{fs} = 2$ and $N_{fb} = 2$.

parameters of the major loop show difference what is consistent with the results of the previous section. At low magnetic flux density, the hysteresis model overestimates the power loss. This is also observed in Fig. 9(b) where the simulated minor loop is wider than the measured loop.

The core power loss P_c was measured in a no load test at 25 °C. In this test, the MFT was supplied from a voltage source converter (VSC) operating at 20 kHz [26]. The power loss was measured with the precision power analyzer ZES Zimmer LMG670. The core power loss P_c measured in the VSC no load test is plotted in Fig. 12. It is compared with the hysteresis power loss P_h calculated based on simulated $B(H)$ with separate hysteresis model parameters and a good fit is observed. The small difference can be explained by different excitation voltages (square voltage in the VSC no load test and sinusoidal voltage in the simulation), neglected eddy current and residual power loss in simulation and uncertainty in the power loss measurement with a square voltage waveform at 20 kHz.

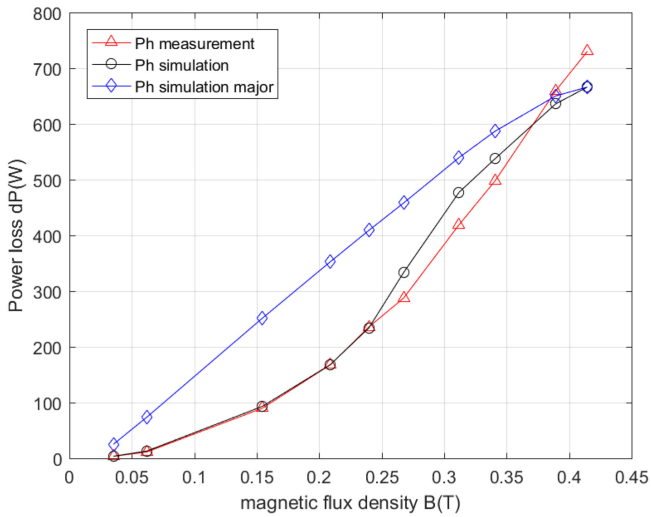

Fig. 11. Core power loss in function of magnetic flux density at 20 kHz and 25 °C according to (5): measured $B(H)$ loop surface (red), simulated $B(H)$ loop surface with separate hysteresis model parameters (black) and simulated $B(H)$ loop surface with major hysteresis loop parameters (blue).

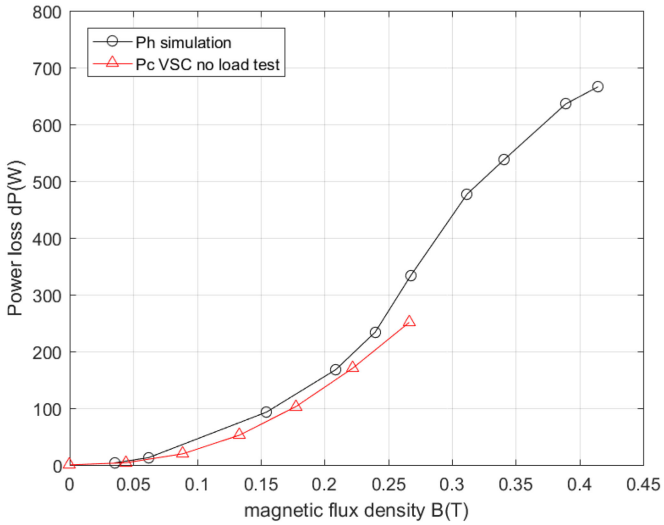

Fig. 12. Core power loss in function of magnetic flux density at 20 kHz and 25 °C: simulated $B(H)$ loop surface according to (5) with separate hysteresis model parameters (black) and measured in the VSC no load test (red).

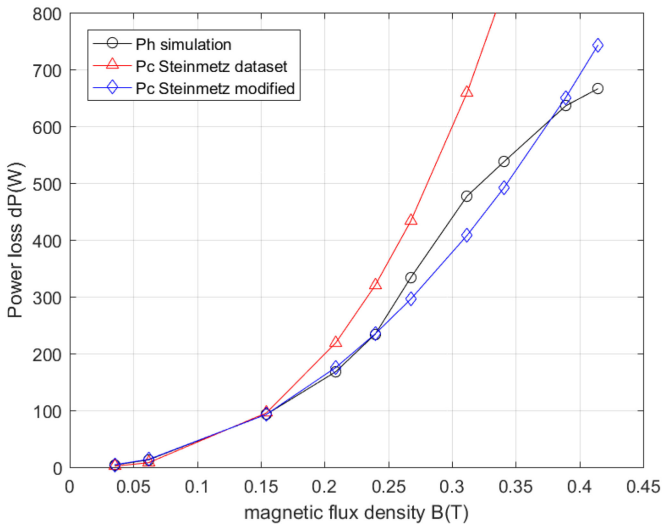

Fig. 13. Core power loss in function of magnetic flux density at 20 kHz and 25 °C: simulated $B(H)$ loop surface according to (5) with separate hysteresis model parameters (black), calculated with IGSE and ferrite datasheet coefficients (red) and calculated with IGSE and proposed coefficients (blue).

The core power loss was calculated with the improved generalized Steinmetz equation (IGSE) [25] and the ferrite material coefficients [63]. The authors highlight that the ferrite material is characterized according to IEC 62044 [59], using a ring core without any air gaps. In Fig. 13 the core power loss P_c is plotted in the function of the magnetic flux density at 20 kHz and at 25 °C. A significant difference is observed above 0.2 T compared to the hysteresis power loss P_h calculated based on simulated $B(H)$. This difference can be explained by the influence of parasitic air gaps [64], neglected eddy current and residual power loss in simulation and accuracy of the ferrite material coefficients at 20 kHz.

Considering that the hysteresis power loss P_h calculated based on simulated $B(H)$ is accurate, then the new set of Steinmetz equation parameters is proposed. The new Steinmetz equation parameters for the multi air gap ferrite core are presented in Table III. The corresponding core power loss P_c is plotted in Fig. 13.

TABLE III
COMPARISON OF STEINMETZ EQUATION PARAMETERS

	Ferrite datasheet [62]	Multi air gap ferrite core
k	3.2	0.60
α	1.46	1.46
β	2.75	2.10

VI. CONCLUSION

The modified Preisach model of hysteresis for a 3-phase medium frequency transformer in a 100 kW DAB converter was presented. The Preisach distribution function is approximated with a two-dimensional Gauss function series and the feedback function is a 3rd-degree polynomial. The measurement of major and minor hysteresis loops was used to determined PDF parameters as well as the number of terms of the Gauss function series, and the number of feedback iterations. The modified Preisach model of hysteresis accurately represents magnetic hysteresis loops in the multi air gap medium frequency transformers composed of type "I" ferrite cores. It has been shown that to accurately model both hysteresis loops (major and minor), parameters for each of them should be determined separately. The assessment of the accuracy of the hysteresis loop model was determined by the relative residual sum of squares, which in both cases is below 0.1%. In the case of a major hysteresis loop, the highest accuracy is obtained for three terms of the Gauss series and one feedback loop. For the correct mapping of a minor loop, only two terms of the Gauss series are significant. In this case, increasing the number of feedback loops improves accuracy. It can be assumed that the first two terms of the Gaussian series are significant for the correct mapping of the hysteresis loop to the saturation point. It is possible to use parameters determined for a major loop to model minor hysteresis loop. The mapping accuracy is acceptable and it is about 1%.

The hysteresis model was used to calculate the core power loss. The power loss calculated based on the hysteresis model was proven accurate compared with the power loss measurement in the transformer no load test. It was shown that in the considered operating conditions, the hysteresis power loss has a major contribution in the overall core power loss. The proposed hysteresis model was used to calculate a new set of Steinmetz equation parameters for the multi air gap ferrite core MFT.

The hysteresis model will be further developed for transient and steady-state circuit simulation of the 3-phase medium frequency transformer. The proposed model could be further extended taking into account a variable number of parasitic air gaps. The influence of the temperature on the hysteresis model parameters should be addressed.

REFERENCES

[1] F. C. Schwarz and J. B. Klaassens, "A controllable 45-kW current source for DC machines," *IEEE Trans. Ind. Appl.*, vol. IA 15, no. 4, pp. 437–444, Jul. 1979.

[2] B. Yang, F. C. Lee, A. J. Zhang, and G. Huang, "LLC resonant converter for front end DC/DC conversion," in *Proc. APEC. 17th Annu. IEEE Appl. Power Electron. Conf. Expo. (Cat. No.02CH37335)*, Mar. 2002, pp. 1108–1112.

[3] L. H. Mweene, C. A. Wright, and M. F. Schlecht, "A 1 kW 500 kHz front-end converter for a distributed power supply system," *IEEE Trans. Power Electron.*, vol. 6, no. 3, pp. 398–407, Jul. 1991.

[4] J. Jacobs, M. Thommes, and R. De Doncker, "A transformer comparison for three-phase single active bridges," in *Proc. Eur. Conf. Power Electron. Appl.*, Dresden, Germany, 2005, p. 10, doi: 10.1109/EPE.2005.219599.

[5] R. W. A. A. De Doncker, D. M. Divan, and M. H. Kheraluwala, "A three-phase soft-switched high-power-density DC/DC converter for high-power applications," *IEEE Trans. Ind. Appl.*, vol. 27, no. 1, pp. 63–73, Jan. 1991.

[6] N. Soltau, H. Stagge, R. W. De Doncker, and O. Apeldoorn, "Development and demonstration of a medium-voltage high-power DC-DC converter for DC distribution systems," in *Proc. IEEE 5th Int. Symp. Power Electron. Distrib. Gener. Syst.*, Jun. 2014, pp. 1–8.

[7] J. Xue, F. Wang, D. Boroyevich, and Z. Shen, "Single-phase vs. three-phase high density power transformers," in *Proc. IEEE Energy Convers. Congr. Expo.*, Sep. 2010, pp. 4368–4375.

[8] M. Mogorovic and D. Dujic, "100 kW, 10 kHz medium-frequency transformer design optimization and experimental verification," *IEEE Trans. Power Electron.*, vol. 34, no. 2, pp. 1696–1708, Feb. 2019.

[9] I. Villar, L. Mir, I. Etxeberria-Otadui, J. Colmenero, X. Agirre, and T. Nieva, "Optimal design and experimental validation of a medium-frequency 400 kVA power transformer for railway traction applications," in *Proc. IEEE Energy Convers. Congr. Expo.*, Sep. 2012, pp. 684–690.

[10] G. Ortiz, J. Biela, D. Bortis, and J. W. Kolar, "1 Megawatt, 20 kHz, isolated, bidirectional 12 kV to 1.2 kV DC-DC converter for renewable energy applications," in *Proc. Int. Power Electron. Conf. Energy Convers. Congr. Expo. ASIA*, Jun. 2010, pp. 3212–3219.

[11] B. Z. Tomczuk, D. Koteras, and A. Waindok, "Electromagnetic and temperature 3-D fields for the modular transformers heating under high-frequency operation," *IEEE Trans. Magn.*, vol. 50, no. 2, pp. 317–320, Feb. 2014.

[12] M. A. Bahmani, "Design considerations of medium-frequency power transformers in HVDC applications," in *Proc. 12th Int. Conf. Ecol. Veh. Renewable Energies*, Apr. 2017, pp. 1–6.

[13] M. Stojadinović and J. Biela, "Modelling and design of a medium frequency transformer for high power DC-DC converters," in *Proc. Int. Power Electron. Conf. Energy Convers. Congr. Expo. Asia*, May 2018, pp. 1103–1110.

[14] M. Mogorovic and D. Dujic, "Medium frequency transformer design and optimization," in *Proc. PCIM Europe Int. Exhib. Conf. Power Electron., Intell. Motion, Renewable Energy Energy Manage.*, May 2017, pp. 1–8.

[15] P. Dworakowski, A. Wilk, M. Michna, B. Lefebvre, F. Sixdenier, and M. Mermet-Guyennet, "Effective permeability of multi air gap ferrite core 3-Phase medium frequency transformer in isolated DC-DC converters," *Energies*, vol. 13, no. 6, Jan. 2020, Art. no. 1352.

[16] Y. Shibuya and S. Fujita, "High frequency model and transient response of transformer windings," in *Proc. IEEE/PES Transmiss. Distrib. Conf. Exhib.*, Oct. 2002, pp. 1839–1844.

[17] M. Dolinar, D. Dolinar, G. Stumberger, B. Polajzer, and J. Ritonja, "A three-phase core-type transformer iron core model with included magnetic cross saturation," *IEEE Trans. Magn.*, vol. 42, no. 10, pp. 2849–2851, Oct. 2006.

[18] F. de Leon and A. Semlyen, "Reduced order model for transformer transients," *IEEE Trans. Power Del.*, vol. 7, no. 1, pp. 361–369, Jan. 1992.

[19] Q. Wu, S. Jazebi, and F. de Leon, "Parameter estimation of three-phase transformer models for low-frequency transient studies from terminal measurements," *IEEE Trans. Magn.*, vol. 53, no. 7, pp. 1–8, Jul. 2017.

[20] P. L. Dowell, "Effects of Eddy currents in transformer windings," *Proc. Inst. Elect. Eng.*, vol. 113, no. 8, pp. 1387–1394, Aug. 1966.

[21] F. Tourkhani and P. Viarouge, "Accurate analytical model of winding losses in round litz wire windings," *IEEE Trans. Magn.*, vol. 37, no. 1, pp. 538–543, Jan. 2001.

[22] M. Xinkui and C. Wei, "More precise model for parasitic capacitances in high-frequency transformer," in *Proc. IEEE 33rd Annu. Power Electron. Specialists Conf. Proc. (Cat. No.02CH37289)*, Jun. 2002, pp. 1054–1057.

[23] Himanshu *et al.*, "High frequency transformer's parasitic capacitance minimization for photovoltaic (PV) high-frequency link-based medium voltage (MV) inverter," *Electronics*, vol. 7, no. 8, Aug. 2018, Art. no. 8.

[24] C. P. Steinmetz, "On the law of hysteresis," *Trans. Amer. Inst. Elect. Eng.*, vol. IX, no. 1, pp. 1–64, Jan. 1892.

[25] K. Venkatachalam, C. R. Sullivan, T. Abdallah, and H. Tacca, "Accurate prediction of ferrite core loss with nonsinusoidal waveforms using only steinmetz parameters," in *Proc. IEEE Workshop Comput. Power Electron.*, Jun. 2002, pp. 36–41.

[26] P. Dworakowski, A. Wilk, M. Michna, A. Fouineau, and M. Guillet, "Lagrangian model of an isolated dc-dc converter with a 3-phase medium frequency transformer accounting magnetic cross saturation," *IEEE Trans. Power Del.*, to be published, doi: 10.1109/TPWRD.2020.2995879.

[27] F. Liorzou, B. Phelps, and D. L. Atherton, "Macroscopic models of magnetization," *IEEE Trans. Magn.*, vol. 36, no. 2, pp. 418–428, Mar. 2000.

[28] A. Wilk, "Representation of magnetic hysteresis in a circuit model of a single-phase transformer," *COMPEL - Int. J. Comput. Math. Elect. Electron. Eng.*, vol. 34, pp. 778–791, May 2015.

[29] D. Dolinar, J. Pihler, and B. Grcar, "Dynamic model of a three-phase power transformer," *IEEE Trans. Power Del.*, vol. 8, no. 4, pp. 1811–1819, Oct. 1993.

[30] J. Tellinen, "A simple scalar model for magnetic hysteresis," *IEEE Trans. Magn.*, vol. 34, no. 4, pp. 2200–2206, Jul. 1998.

[31] E. C. Stoner and E. P. Wohlfarth, "A mechanism of magnetic hysteresis in heterogeneous alloys," *Philos. Trans. R. Soc. Lond. Ser. Math. Phys. Sci.*, vol. 240, no. 826, pp. 599–642, May 1948.

[32] A. Globus, "Universal hysteresis loop for soft ferromagnetic materials," in *Proc. Eur. Phys. Soc. Conf. Soft Magn. Mater.*, 1975, p. 233.

[33] D. Jiles and D. Atherton, "Ferromagnetic hysteresis," *IEEE Trans. Magn.*, vol. 19, no. 5, pp. 2183–2185, Sep. 1983.

[34] F. Preisach, "Über die magnetische nachwirkung," *Z. Für Phys.*, vol. 94, no. 5, pp. 277–302, May 1935.

[35] G. Xue, P. Zhang, Z. He, D. Li, Z. Yang, and Z. Zhao, "Modification and numerical method for the jiles-atherton hysteresis model," *Commun. Comput. Phys.*, vol. 21, no. 3, pp. 763–781, Mar. 2017.

[36] A. Ivani, J. Fuzi, and Z. Szabo, "Preisach models of ferromagnetic hysteresis," *Przeglad Elektrotechniczny*, vol. R. LXXIX 3/2003, pp. 145–150, 2003.

[37] C. Jedryczka, P. Sujka, and W. Szelag, "The influence of magnetic hysteresis on magnetorheological fluid clutch operation," *COMPEL Int. J. Comput. Math. Elect. Electron. Eng.*, vol. 28, pp. 711–721, May 2009.

[38] W. Łyskawinski, P. Sujka, W. Szelag, and M. Baranski, "Numerical analysis of hysteresis loss in pulse transformer," *Arch. Elect. Eng.*, vol. 60, pp. 187–195, 2011.

[39] J. Gyselinck, P. Dular, N. Sadowski, J. V. Leite, and J. P. A. Bastos, "Incorporation of a jiles-atherton vector hysteresis model in 2D FE magnetic field computations: Application of the newton-raphson method," *COMPEL Int. J. Comput. Math. Elect. Electron. Eng.*, vol. 23, pp. 685–693, Sep. 2004.

[40] M. A. Krasnosel'skii and A. V. Pokrovskii, *Systems With Hysteresis*. Berlin Heidelberg: Springer-Verlag, 1989.

[41] I. Mayergoyz, "Mathematical models of hysteresis," *IEEE Trans. Magn.*, vol. 22, no. 5, pp. 603–608, Sep. 1986.

[42] G. Kadar and E. Torre, "Hysteresis modeling: I Non-congruency," *IEEE Trans. Magn.*, vol. 23, no. 5, pp. 2820–2822, Sep. 1987.

[43] M. Brokate and E. Della Torre, "The wiping-out property of the moving model (magnetic hysteresis)," *IEEE Trans. Magn.*, vol. 27, no. 5, pp. 3811–3814, Sep. 1991.

[44] I. D. Mayergoyz and A. A. Adly, "Numerical implementation of the feedback preisach model," *IEEE Trans. Magn.*, vol. 28, no. 5, pp. 2605–2607, Sep. 1992.

[45] E. Della Torre and F. Vajda, "Parameter identification of the complete-moving-hysteresis model using major loop data," *IEEE Trans. Magn.*, vol. 30, no. 6, pp. 4987–5000, Nov. 1994.

[46] C. Ragusa, "An analytical method for the identification of the Preisach distribution function," *J. Magnetism Magn. Mater.*, vol. 254/255, pp. 259–261, Jan. 2003.

[47] O. Henze and W. M. Rucker, "Identification procedures of Preisach model," *IEEE Trans. Magn.*, vol. 38, no. 2, pp. 833–836, Mar. 2002.

[48] M. Brokate, "Some mathematical properties of the Preisach model for hysteresis," *IEEE Trans. Magn.*, vol. 25, no. 4, pp. 2922–2924, Jul. 1989.

[49] A. Bilski and M. Twardy, "Hysteresis modeling using a preisach operator," *Int. J. Electron. Telecommun.*, vol. 56, no. 4, pp. 473–478, 2010.

[50] M. Luo, D. Dujic, and J. Allmeling, "Modeling frequency independent hysteresis effects of ferrite core materials using permeance–capacitance analogy for system-level circuit simulations," *IEEE Trans. Power Electron.*, vol. 33, no. 12, pp. 10055–10070, Dec. 2018.
[51] P. Dworakowski, A. Wilk, and B. Lefebvre, "Hysteresis modelling of a medium frequency single-phase transformer," in *Proc. 19th Eur. Conf. Power Electron. Appl.*, Sep. 2017, pp. P.1–P.9.
[52] P. Dworakowski, A. Wilk, M. Michna, B. Lefebvre, and T. Lagier, "3-phase medium frequency transformer for a 100 kW 1.2 kV 20 kHz dual active bridge converter," in *Proc. IEEE IECON 45th Annu. Conf. Ind. Electron. Soc.*, Oct. 2019, pp. 4071–4076.
[53] T. Nakata, N. Takahashi, and Y. Kawase, "Magnetic performance of step-lap joints in distribution transformer cores," *IEEE Trans. Magn.*, vol. 18, no. 6, pp. 1055–1057, Nov. 1982.
[54] N. Hihat, E. Napieralska-Juszczak, J.-P. Lecointe, J. K. Sykulski, and K. Komeza, "Equivalent permeability of step-lap joints of transformer cores: Computational and experimental considerations," *IEEE Trans. Magn.*, vol. 47, no. 1, pp. 244–251, Jan. 2011.
[55] P.-S. Shin and J. Lee, "Magnetic field analysis of amorphous core transformer using homogenization technique," *IEEE Trans. Magn.*, vol. 33, no. 2, pp. 1808–1811, Mar. 1997.
[56] A. Ayachit and M. K. Kazimierczuk, "Sensitivity of effective relative permeability for gapped magnetic cores with fringing effect," *IET Circuits Devices Amp. Syst.,* vol. 11, no. 3, pp. 209–215, Jan. 2017.
[57] E. F. Fuchs and Y. You, "Measurement of $\lambda-1$ characteristics of asymmetric three-phase transformers and their applications," *IEEE Power Eng. Rev.*, vol. 22, no. 8, pp. 69–70, Aug. 2002.
[58] Ferroxcube. "3C90 material specification," Accessed: Jan. 19, 2020. [Online]. Available: https://www.ferroxcube.com/upload/media/product/file/MDS/3c90.pdf
[59] "IEC 62044 cores made of soft magnetic materials - measuring methods." Accessed: May 08, 2020. [Online]. Available: https://webstore.iec.ch/publication/6349
[60] "Unconstrained nonlinear optimization algorithms - MATLAB & simulink," Accessed: May 22, 2020. [Online]. Available: https://www.mathworks.com/help/optim/ug/unconstrained-nonlinear-optimization-algorithms.html#f3137
[61] A. Wilk, M. Michna, and A. Cichowski, "Simulation of the remanence influence on the transient states of the single-phase transformer including feedback Preisach model," in *Proc. IEEE IECON 40th Annu. Conf. Ind. Electron. Soc.*, Oct. 2014, pp. 875–880.
[62] A. Fujita, H. Kobiki, and S. Gotoh, "Relationship between residual loss and hysteresis loss of mnzn ferrites," *J. Magn. Soc. Jpn.*, vol. 22, no. S_1_ISFA_97, pp. S1_286–S1_288, 1998.
[63] Ferroxcube. "Design of planar power transformer," Accessed: Jun. 01, 2020. [Online]. Available: http://ferroxcube.home.pl/appl/info/plandesi.htm
[64] A. Ayachit and M. K. Kazimierczuk, "Steinmetz equation for gapped magnetic cores," *IEEE Magn. Lett.*, vol. 7, pp. 1–4, Mar. 2016.